# Synthetic genetic elements enable rapid characterization of inorganic carbon uptake systems in *Cupriavidus necator* H16

**Akira K. Nakamura[1,2], Emily M. Fulk[3], Christopher W. Johnson[3], and Farren J. Isaacs*[1,2,4]**

[1] Department of Molecular, Cellular & Developmental Biology, Yale University, New Haven, CT 06520, USA
[2] Systems Biology Institute, Yale University, West Haven, CT 06516, USA
[3] Renewable Resources and Enabling Sciences Center, National Renewable Energy Laboratory, Golden, CO 80401, USA
[4] Department of Biomedical Engineering, Yale University, New Haven, CT 06520, USA

*Correspondence should be addressed to: FJI (farren.isaacs@yale.edu) - +1-203.737.3156

## Abstract

*Cupriavidus necator* H16 is a facultative chemolithotroph capable of using $CO_2$ as a carbon source, making it a promising organism for carbon-negative biomanufacturing of petroleum-based product alternatives. In contrast to model microbes, genetic engineering technologies are limited in *C. necator*, constraining its utility in basic and applied research. Here, we developed a genome engineering technology to efficiently mobilize, integrate, and express synthetic genetic elements (SGEs) in *C. necator*. We tested the chromosomal expression of four inducible promoters to optimize an engineered genetic landing pad for tunable gene expression. To demonstrate utility, we employed the SGE system to design, mobilize, and express eight heterologous inorganic carbon uptake pathways in *C. necator*. We demonstrated all inorganic carbon uptake systems upregulated intracellular bicarbonate concentrations under heterotrophic conditions. This work establishes the utility of the SGE strategy for expedited integration and expression of heterologous pathways and enhances intracellular bicarbonate concentrations in *C. necator*.

**Keywords:** Cupriavidus necator, Genome engineering, Chromosomal integration, Inducible promoter, Inorganic carbon uptake, CCM

## Introduction

The global challenge of mitigating climate change has intensified the search for sustainable methods of producing materials traditionally derived from petroleum. These materials, such as plastics, synthetic fibers, and chemicals, are essential in modern society but contribute significantly to greenhouse gas (GHG) emissions through the energy-intensive polymerization processes, petroleum extraction and refining, and incineration[1]. Biomanufacturing, a process in which biological systems are utilized to produce valuable compounds from renewable resources, offers a promising alternative to conventional fossil fuel-based production methods[2–4]. Further, recent studies have demonstrated there is potential to offset carbon emissions in the process of producing bio-based alternatives by employing microbes capable of utilizing GHGs, such as $CO_2$ and $CH_4$, as carbon sources[5,6].

The facultative chemolithotroph *Cupriavidus necator* is a promising candidate for carbon-negative biomanufacturing[7,8]. Initially recognized for its native ability to produce and accumulate high titers of polyhydroxybutyrate (PHB), *C. necator* has since been engineered to produce a wide range of high-value compounds[9–18]. This metabolic versatility combined with its ability to use $CO_2$ as a carbon source make it a promising candidate organism for sustainable bioproduction. However, compared to model organisms (e.g., *Escherichia coli*), *C. necator* physiology is less understood, and its genetic toolkit remains limited[8,19]. Expanding this toolkit is a crucial step toward advancing *C. necator* as an industrial microbe. Specifically, advancing *C. necator* as a biomanufacturing chassis requires tools for efficient design, mobilization, and chromosomal integration of synthetic genetic elements (SGEs). Achieving robust heterologous expression of multi-gene pathways, such as those involved in metabolic diversification, demands integration technologies capable of accommodating large genetic constructs with minimal workflow complexity.

Currently, the most utilized chromosomal integration method in *C. necator* consists of selection and counter-selection for homologous recombination (HR) driven crossover events[20,21]. Although this method is adept for generating marker-free genomic integrations, it is less conducive to rapid prototyping of metabolic pathways due to the lengthy generation timeline and limited frequency of recombination, which subsequently limits throughput. Four rounds of re-streaking are typically required to confirm the double-crossover, which amounts to a minimum

of 10 days from conjugation if colonies form with the typical incubation of 2 days. The method is also limited by the length of the integration cargo due to decreased integration efficiency for larger (>5 kb) fragments[22]. Further, transposition-based methods are versatile but can lead to site-dependent expression variability due to the influence of local genomic context on gene expression and disruption of essential genetic elements[23,24]. These limitations in the current genetic toolkit for *C. necator* highlight the need for more efficient chromosomal integration tools. Adapting a landing-pad based integration strategy for *C. necator* could significantly enhance our ability to optimize both heterologous and native metabolic pathways by accelerating the design-build-test-learn cycle[25,26].

As a potential chassis for carbon-negative biomanufacturing, *C. necator* can fix carbon through the Calvin-Benson-Bassham (CBB) cycle, with ribulose-1,5-bisphosphate carboxylase/oxygenase (Rubisco) catalyzing the key carboxylation reaction. However, Rubisco's carboxylation efficiency is limited by its inability to effectively discriminate between $CO_2$ and $O_2$, leading to competing oxygenation[27]. While the *C. necator* Rubisco exhibits higher specificity for $CO_2$ over $O_2$ relative to other Rubisco homologs, this comes at the cost of a lower catalytic rate ($K_{cat}$), resulting in slow growth under atmospheric $CO_2$ levels[28,29]. In contrast, cyanobacteria and some chemolithotrophs have Rubisco species exhibiting higher carboxylation rates, which they achieve using $CO_2$-concentrating mechanisms (CCMs) that increase the $CO_2$-to-$O_2$ ratio in close proximity of Rubisco[30]. CCMs typically involve inorganic carbon (Ci) uptake systems, such as bicarbonate transporters and $CO_2$-to-$HCO_3^-$ vectorial conversion complexes, to increase intracellular Ci levels[31,32]. Recent studies have shown that expressing the *Halothiobacillus neapolitanus* DAB2 and cyanobacterial SbtAB Ci uptake systems in *C. necator* can enhance intracellular bicarbonate levels under ambient $CO_2$ concentrations, illustrating the potential for future engineering of *C. necator's* carbon fixation pathways for improved autotrophic growth[33,34].

In this study, we adapted the SGE mobilization scheme from Patel & Oh *et al.* (2022) for *C. necator*-specific expression and utilized it to chromosomally integrate and express a range of Ci uptake systems in *C. necator* (**Figure 1**)[25]. We tested the chromosomal expression of four inducible promoter systems, previously only characterized in *C. necator* episomally[35,36]. By leveraging an engineered high $CO_2$-requiring (HCR) phenotype, we assessed the ability of these

Ci uptake systems to increase intracellular bicarbonate concentrations and restore growth under ambient $CO_2$ levels. This novel characterization of four Ci uptake systems in *C. necator* under heterotrophic conditions contributes to future CCM engineering efforts. Ultimately, we anticipate that our technology will accelerate the optimization and diversification of genetic modifications and metabolite production in *C. necator*.

## Results

### Testing SGE mobilization scheme in *Cupriavidus necator*

To develop an efficient chromosomal integration strategy in *C. necator*, we tested the broad host range SGE mobilization approach developed in Patel & Oh *et al.* (2022)[25]. The integration methodology comprised of three main steps: (1) conjugation-mediated random transposition of a landing pad cassette into the host genome, (2) identification of genomic sites conducive to ectopic expression, and (3) targeted integration of SGEs at identified sites (**Figure 1**). The pLP vector drives random transposition of the landing pad cassette into the genome via activity of the Mariner family Himar transposase. Within the landing pad, a T7 RNA polymerase (T7 RNAP) circuit drives GFP expression (**Figure 2A**). The T7 RNAP circuit transcriptionally and translationally regulates T7 RNAP expression with a TetR repressor and theophylline riboswitch. Expression levels from the T7 RNAP circuit are controlled by the concentration of the respective inducers, anhydrotetracycline (aTc) and theophylline.

Conjugation and transposition of the landing pad cassette into wild-type *C. necator* was successful, exhibiting transconjugation frequencies of ~$4.2 \times 10^{-7}$ (**Figure 2B**). Following transposition, we analyzed ~10,000 clones of the transposed population for GFP expression from the landing pad using flow cytometry. This fluorescence serves as a proxy for gene expression from the inserted locus, and aids in identifying genomic safe harbors for robust and tunable gene expression. The transposed population demonstrated broad fluorescence distributions evidenced by an elevated coefficient of variation (CV) (**Figure 2C**). We hypothesized that the high CV is a result of variable gene expression observed across population due to locus-dependent context effects[23,25,37,38]. To further characterize these context effects, we analyzed three individual clones on the plate reader and with flow cytometry. Although each clone demonstrated different

absolute levels of fluorescence, the fold change between uninduced and induced expression was consistently ~4-fold (**Figure 2C, D**).

In the absence of aTc and theophylline, the population exhibited moderate fluorescence levels of $1.3 \times 10^2$ A.U. (**Figure 2C**), indicating an elevated level of basal expression. We hypothesized the elevated basal expression was an artifact of inefficient repression from either or both forms of negative regulation. Clones treated with only aTc and clones treated with only theophylline demonstrated similar levels of fluorescence (**Figure 2E**), indicating the elevated basal expression was not strongly attributed to one form of regulation over another. We further subjected clones to increasing concentrations of one inducer, while keeping the concentration of the other inducer constant. From this experiment, we observed a) 1.8-to-2.5-fold increase in normalized fluorescence between no aTc and 100 ng/mL aTc conditions and b) 2.6-to-3.9-fold increase between no theophylline and 1 mM theophylline conditions (**Figure 2E**). These results show that both forms of regulation individually repress T7 RNAP activity inefficiently. Further, our observations of the TetR repressor align with a previous study in *C. necator* that reported similar incomplete repression of expression from TetR/$P_{rrsC\text{-}tetO}$ systems[39]. These findings indicate a need to modify the landing pad system to achieve tighter repression and greater dynamic range in *C. necator*.

## Optimizing SGE mobilization scheme for optimal expression in *Cupriavidus necator*

We adapted the landing pad for *C. necator*-specific expression by replacing the T7 RNAP circuit with inducible promoters that have previously been characterized in *C. necator* for episomal expression. Specifically, we tested the widely used cross-species arabinose (AraC/$P_{araBAD}$) and rhamnose (RhaRS/$P_{rhaBAD}$) inducible promoter systems, as well as the *C. necator*-derived salicylate (NahR/$P_{H16\_RS08125}$) and benzoate (BenM/$P_{H16\_RS09790}$) inducible systems[36]. Both the arabinose and rhamnose inducible systems have a large dynamic range when expressed episomally from the pBBR1 broad host range origin in *C. necator* and are the benchmarking standard for evaluating new inducible promoters[35,36,40]. The salicylate and benzoate inducible promoters have been reported to mediate inductions of 292- and 403-fold in *C. necator*, respectively[36]. Further, the benzoate induced absolute normalized fluorescence was reported to be >11-fold higher than AraC/$P_{araBAD}$ when expressed from the pBBR1 origin in *C. necator*[36].

We constructed landing pad variants with these inducible promoters driving GFP reporter expression (**Figure 3A**) and introduced them into wild-type *C. necator* and the ΔH16_A006 restriction enzyme (RE) Δ*phaCAB* background. The ΔRE background is commonly used in metabolic engineering applications, because deletion of the *H16_A0006* restriction enzyme-encoding gene has been demonstrated to increase electroporation efficiency by ~1,600-fold in comparison to electroporation efficiency into wild type *C. necator*[41]. Further, removing the *phaCAB* operon prevents PHB accumulation prevalent under nutrient limitation[42,43]. Landing pad integrant populations were analyzed with flow cytometry to observe the fluorescence distribution of each system. All induced systems were treated with 5 mM of the respective inducer based on previous studies in *C. necator*[35,36]. In both backgrounds, the arabinose inducible system demonstrated the strongest activation of *gfp* with 165- and 118-fold induction in wild type and ΔREΔ*phaCAB*, respectively (**Figure 3B and S1)**. The rhamnose inducible system demonstrated the lowest uninduced expression leading to 135- and 86-fold induction in wild type and ΔREΔ*phaCAB*, respectively. The salicylate inducible system demonstrated 58- and 63-fold induction, and the benzoate inducible system demonstrated 5- and 40-fold induction in wild type and ΔRE Δ*phaCAB*, respectively. For the salicylate and benzoate inducible systems, we also observed that the maximum $OD_{600}$ was greater in induced clones than in uninduced clones (**Figure S2**), and fluorescence levels of the induced clones decreased ~5-8 hours post induction (**Figure S3**). These results suggest that *C. necator* metabolizes sodium salicylate and sodium benzoate, thereby depleting the media of available inducer, as previously observed in Hanko *et al.* (2020).

We proceeded to screen the ΔREΔ*phaCAB*.$P_{araBAD}$LP and ΔREΔ*phaCAB*.$P_{rhaBAD}$LP populations for clones with landing pad integration into a locus accommodating dynamic expression. Screening 192 clones per population revealed four candidates with high GFP expression for each landing pad variant (**Figure 3C**). These candidates were evaluated across a range of inducer concentrations, confirming minimal uninduced expression and substantial dynamic range (**Figure 3D**). Clones demonstrated a maximum of 46- and 33-fold induction for the arabinose and rhamnose systems, respectively.

We further identified the genomic sites of $P_{araBAD}$ landing pad integration for 7 clones from the ΔREΔ*phaCAB*.$P_{araBAD}$LP population (Table S1). Whole genome sequencing revealed

that clones varied in integration site and landing pad copy number. Integration sites were observed in TA dinucleotides across the two chromosomes and the pHG1 megaplasmid. Multiple integration events of the $P_{araBAD}$LP were observed in 4 of the 7 clones, with a maximum of 3 copies identified in a single clone. These results highlight the role of context effects and copy number in determining amplitude and variability of expression levels from the landing pad. Further, the strain with the highest fold change in fluorescence in response to l-arabinose induction, from a single integration site, had the landing pad in the coding region of a SDR (short-chain dehydrogenases/reductases) family NAD(P)-dependent oxidoreductase on chromosome 1, 2 Mb downstream of the origin of replication. Together, these results guided the selection of clones for further study, prioritizing those with single-site integrations and high induction dynamic range.

## Identifying inorganic carbon uptake systems that elevate intracellular inorganic carbon concentrations in *C. necator*

Having validated the SGE technology with dynamic expression profiling of inducible systems, we next applied this framework to evaluate heterologous Ci uptake systems. These systems, sourced from diverse organisms, were tested for their capacity to enhance intracellular dissolved inorganic carbon (DIC) levels in *C. necator*, leveraging the SGE method for precise and high-throughput assessment. Six Ci uptake systems were identified from the literature for expression in *C. necator* (**Table 1**)[44–46]. Heterologous expression of these diverse complexes have been demonstrated to increase intracellular DIC levels in *E. coli*[44,46]. Additionally, previous studies have also shown *H. neapolitanus* DAB2 and Cyanobacterial SbtA to increase intracellular concentrations of bicarbonate in *C. necator* and therefore we included these systems as positive controls[33,34].

To establish a functional readout for Ci uptake activity of the candidate Ci systems in *C. necator*, we engineered an HCR phenotype. Bicarbonate is an essential substrate, not only in facilitating the CBB cycle, but also in core metabolic processes such as the TCA cycle, nucleotide, and lipid synthesis[47]. At atmospheric $CO_2$ concentrations (~0.04%), the spontaneous hydration of $CO_2$ does not supply sufficient levels of bicarbonate to sustain these central reactions. Carbonic anhydrases (CAs), which catalyze $CO_2$-bicarbonate conversion, help meet

this demand. Previous studies identified four CAs in *C. necator*, and deleting the CA *can* gene was shown to induce an HCR phenotype[33,34,48].

We leveraged this phenotype to determine if the candidate Ci uptake systems could increase intracellular bicarbonate to levels sufficient for growth in HCR *C. necator* under ambient air conditions (**Figure 4A**). The *can* deletion mutant was constructed in the ΔREΔ*phaCAB* background and successful deletion was confirmed by clonal PCR screens using primers that amplify across the locus (**Figure 4B**)[20,49]. Growth assays supported prior findings, showing that the *can* knockout failed to grow under atmospheric $CO_2$ but thrived in elevated $CO_2$ (**Figure 4C**). To enable chromosomal integration of the Ci candidates, we transposed the arabinose inducible landing pad ($P_{araBAD}$LP) into the HCR ΔREΔ*phaCAB* Δ*can* strain. We isolated a clone demonstrating 13-fold induction in fluorescence as the background strain for Ci uptake system expression (**Figure 4D**). This clone was confirmed to have a single copy of the arabinose inducible landing pad in chromosome 1 (**Table S1**).

## Landing pad expression of inorganic carbon uptake systems recover high $CO_2$-requiring phenotype in *C. necator*

To integrate the Ci uptake system candidate pathways into the landing pad, the respective SGEs were assembled into the pPath vector. The pPath vector harbors the serine recombinase, PhiC31, which can catalyze recombinase mediated cassette exchange (RMCE) between pairs of noncomplementary attP and attB recognition sites[25,50]. Transformation of the pPath vector, followed by induced transcription of the PhiC31 integrase, drives the attB-site flanked SGEs to displace the attP-site flanked GFP reporter in the landing pad.

pPath-Ci uptake system plasmids were conjugated into the ΔREΔ*phaCAB*Δ*can*$P_{araBAD}$LP strain, where Ci uptake systems were integrated into the landing pad via PhiC31 integrase mediated cassette exchange (**Figure 5A, B**). Integrated strains were then subjected to titrated concentrations of arabinose between 0 and 15 mM and cultured overnight under ambient $CO_2$ concentrations. Growth measurements were taken 22 hours post induction with a plate reader. All Ci uptake system-expressing strains demonstrated growth, indicating that the expression of these uptake systems increased intracellular bicarbonate concentrations to levels required for

anabolism (**Figure 5C**). The induction condition demonstrating the maximum $OD_{600}$ was 1 mM arabinose for strains expressing the *H. neapolitanus* Dab2 and SbtA homologs, and 5 mM arabinose for strains expressing *Am. ferrooxidans*-, *At. ferrooxidans*-, *H. crunogenus*-, *Sulfurovum sp. AR*-, and *T. ruber*-derived Ci uptake systems. The highest $OD_{600}$ for all strains were comparable to the $OD_{600}$ of the ancestral ΔREΔ*phaCAB* strain. These findings first provided evidence that candidate Ci uptake system expression from the landing pad at these induction conditions were sufficient for restoring Δ*can* growth to levels comparable to the native presence of *can*. Moreover, treatment with higher concentrations of inducer did not significantly enhance or diminish $OD_{600}$ in comparison to the optimal inducer concentrations. Given that $P_{araBAD}$-driven GFP expression from the landing pad did not plateau at these arabinose concentrations in the ΔREΔ*phaCAB* background (**Figure 3D**), this constancy of OD at higher inducer concentrations suggested that further increase in intracellular bicarbonate concentration did not improve heterotrophic growth and slight excess in bicarbonate was not detrimental to growth. Overall, these results indicated that the tested Ci uptake systems were sufficient at meeting the metabolic demand for bicarbonate under heterotrophic conditions.

## Discussion

In this study, we advanced the state-of-the-art in genome engineering in *C. necator* by developing an efficient and reliable SGE mobilization scheme that allows tunable expression of chromosomal-based pathways. Utilizing this approach, we demonstrated the chromosomal expression of eight heterologous Ci uptake systems and demonstrated their ability to increase intracellular bicarbonate concentration in *C. necator*, which can support future efforts to reconstitute *bona fide* CCMs. This work helps facilitate the development of chromosomal integration strategies in *C. necator*, marking a shift from traditional HR-mediated methods to more versatile and efficient approaches[7,20,51,52].

The SGE mobilization technology addresses several shortcomings and limitations faced with the selection/counterselection method. First, the landing pad-based strategy minimizes heterologous expression workload and accelerates integrant generation timelines in comparison to the homologous recombination-enabled selection/counter-selection method. Following landing pad integration, our *C. necator* strains are ready for chromosomal integration ‘off-the-shelf’,

with the post conjugation workflow being reduced by 75% to a single round of selection with a timeline of two days. This comparative conservation of eight days enables more rounds of integration and testing within the same timeframe, making this method more adept for pathway diversification and optimization. Additionally, our landing pad design enables identification of integration loci accommodating robust cargo expression, beyond the handful of previously characterized sites[19]. By assessing promoter activity in the integration locus with a GFP reporter prior to cargo integration, our system allows empirical selection of favorable integration sites that demonstrate a dynamic range in expression. To develop marker-less integrations that do not require additional transformations, future work could focus on developing self-excising recombination cassettes. Second, chromosomal integration via PhiC31 RMCE overcomes fragment size limitations observed with HR-mediated integration methods in organisms with low endogenous HR efficiency[22]. Serine recombinases are not constrained by host factors and mediate site-specific recombination between defined attP and attB sequences, with precedent of integrations as large as 133 kb in Drosophila[50]. This mechanism is compatible with large fragment integrations because it is independent of homology processing and endogenous machinery. To realize multi-pathway integrations with orthogonal landing pads, it will be integral to expand the repertoire of available integrase-att site pairs and characterize RMCE activity of known integrases in *C. necator*.

Characterization of inducible promoters from the *C. necator* chromosome demonstrate that characterizations conducted on plasmid-based systems cannot be directly extrapolated to chromosomal contexts. The inducible promoters we express at 1 to 3 copies were previously characterized on the medium copy ori, pBBR1 (~40 copies per cell)[35,36,53]. We observed a smaller fold-change in induction with our chromosomally expressed inducible promoters in comparison to these previous plasmid-based studies. We hypothesize that this reduced fold change in induction arises from the multiplicative scaling effect, where induced expression levels are amplified more than uninduced levels in higher-copy systems, resulting in a greater apparent fold-change compared to lower-copy systems. We also showed that expressing heterologous pathways from different genomic locations has a significant effect on absolute expression level. Given that carbon-negative biomanufacturing applications will utilize more physiologically relevant chromosomal gene expression due to factors such as stability and inability to use antibiotics in commercial-scale processes, our findings illustrate the importance of characterizing

genetic parts in a chromosomal context[54]. Strategies such as utilizing RBSs with greater ribosomal affinity and introducing multiple chromosomal copies of a given gene can be implemented to further increase expression.

Further, while this manuscript was in review, Federici *et al.* published CIFR (clone-integrate-flip-out-repeat), a complementary homologous recombination-independent genome integration method demonstrated in three gram-negative bacteria, including *C. necator*[52]. Both the CIFR workflow and our approach utilize transposon-driven random genomic integration for an empirically informed selection of integration sites. On the other hand, the CIFR workflow employed an integrase excision scheme to achieve iterative genomic integration of cargo with minimal integration of unwanted genetic material, while our approach utilized a landing pad scheme for accelerated and higher throughput testing of various pathway candidates. We believe that integrating these two strategies could allow for a more efficient and accessible genome integration approach in *C. necator* and other gram-negative bacteria.

Advances in genome engineering technologies are essential in performing rapid functional genomics or fully realizing carbon-negative biomanufacturing using *C. necator*. For example, recent studies have successfully demonstrated gene deletions using CRISPR/Cas9 and transient gene knock downs using CRISPR inference[41,55,56]. However, the *E. coli* genetic toolkit presents many more tools that can be applied in *C. necator* to probe a greater variety of genomic modifications. For example, adaptation of an oligo recombineering technique like MAGE (multiplexed automated genome engineering) would enable rapid diversification of native metabolic pathways for directed evolution and pathway engineering[57,58]. Additionally, heterologous pathways could be diversified with MAGE in *E. coli* and mobilized into the *C. necator* genome using the SGE mobilization technology. Such methods could be utilized to enhance $CO_2$ fixation capabilities in *C. necator*, improving its utility as a host for converting $CO_2$ to valuable metabolic products.

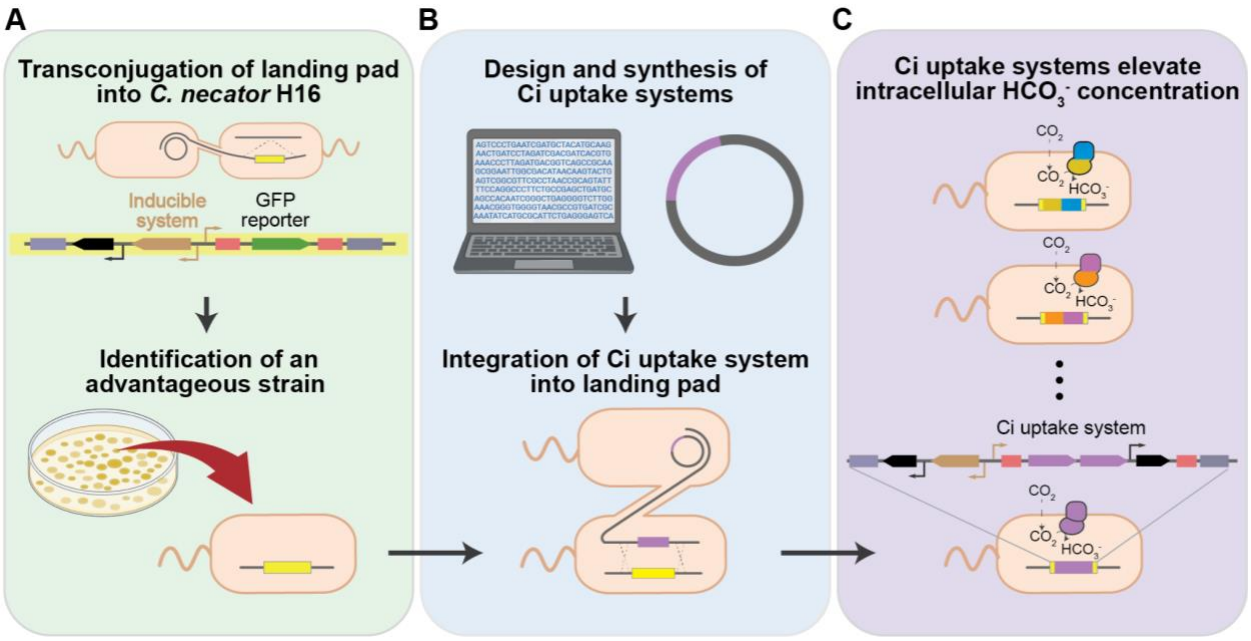


**Figure 1. Design, synthesis, and mobilization of synthetic genetic elements for rapid expression and characterization in *C. necator*.** (A) Landing pad cassette is randomly integrated into the *C. necator* genome via Himar transposase activity. The cassette harbors an inducible expression system driving expression of a GFP reporter. GFP expression profiles are used as a proxy for selecting clones with integration in a desirable locus. B) Designed and synthesized Ci uptake system-encoding genes are assembled between attB sites on the pPath vector. PhiC31 integrase expression from the pPath vector directs displacement of the attP site-flanked GFP reporter with the Ci uptake system pathways. (C) Ci uptake system pathways are chromosomally integrated into the characterized landing pad locus and ready for tunable expressed for further characterization.

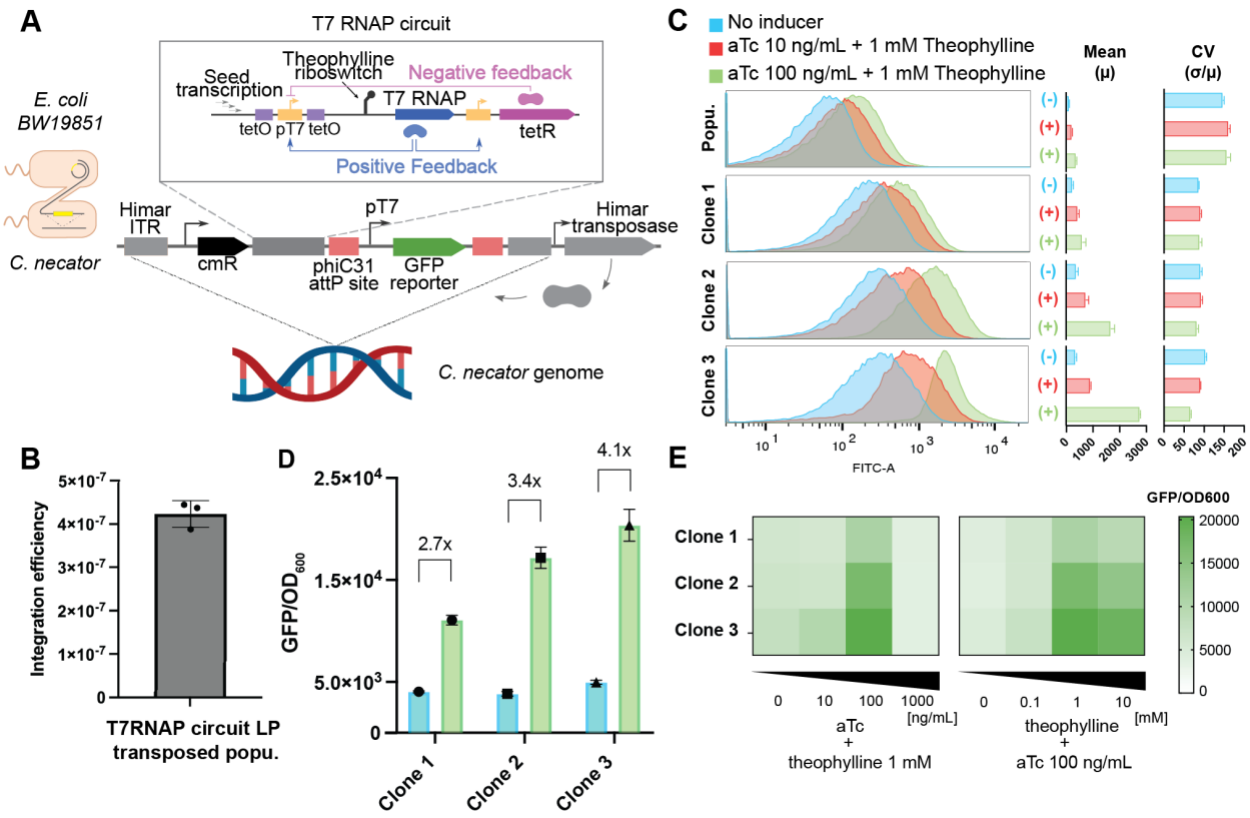


**Figure 2. Developing SGE mobilization technology in *C. necator*.** (A) Schematic of landing pad. Coupled conjugation-transposition is used to deliver a landing pad into *C. necator* genome. The *cmR* gene allows chloramphenicol selection of strains with landing pad integration. PhiC31 integrase attP sites flank the pT7-GFP reporter for RMCE in subsequent conjugation of genetic payload. (B) Transconjugation efficiency of T7 RNAP circuit landing pad population. (C) ~10,000 clones containing the T7 RNAP circuit landing pad in the *C. necator* H16 background were pooled and assayed for fluorescence by flow cytometry. Fluorescence distribution of uninduced (blue) and induced (red, aTc 10 ng/mL + 1 mM theophylline; green, aTc 100 ng/mL + 1 mM theophylline) cells was quantified. Three individual clones were randomly picked and similarly quantified with and without induction. Mean and coefficient of variation (CV) are shown to quantify expression strength and variability, respectively. Cell counts represented in the y-axis were normalized to mode. (D) GFP induction of individual clones was quantified on a plate reader, fluorescence collected for 20 h after 1 mM theophylline and 100 ng/mL aTc induction (green) and no induction (blue). (E) Fluorescence in response to increasing concentration to either aTc or theophylline was collected on a plate reader 20 h after induction. For each titration experiment, the non-titrated inducer was constant at 1 mM for theophylline and 100 ng/mL for aTc. Heatmap represents the average value of replicates.

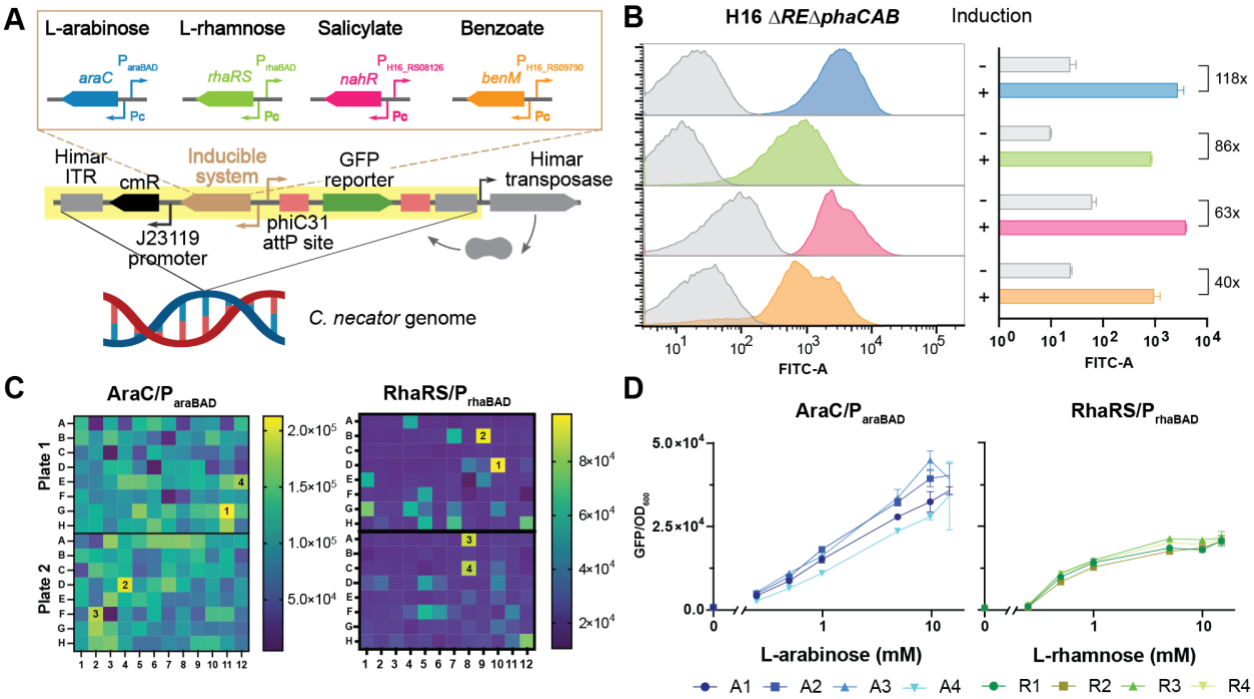


**Figure 3. Landing pad expression optimized for *C. necator*.** (A) Schematic of landing pad with inducible promoter candidates replacing the T7 RNAP circuit. (B) ~50,000 clones containing the landing pad variants in the *C. necator H16* ΔREΔ*phaCAB* background were pooled and assayed for fluorescence (FITC-A) by flow cytometry. Fluorescence distribution of uninduced (gray) and induced (5mM of respective inducer; blue: l-arabinose; green: l-rhamnose; pink: sodium salycilate; orange: sodium benzoate) cells was quantified. (C) 192 random colonies/population from the AraC/$P_{araBAD}$ and RhaRS/$P_{rhaBAD}$ landing pad populations were picked and assayed for fluorescence with a plate reader 20 h post induction with 5 mM of respective inducer. (D) Four clones demonstrating the highest fluorescence were selected from (C) and subjected to increasing concentrations of the respective inducer. Fluorescence was assayed 20 h post induction using a plate reader.

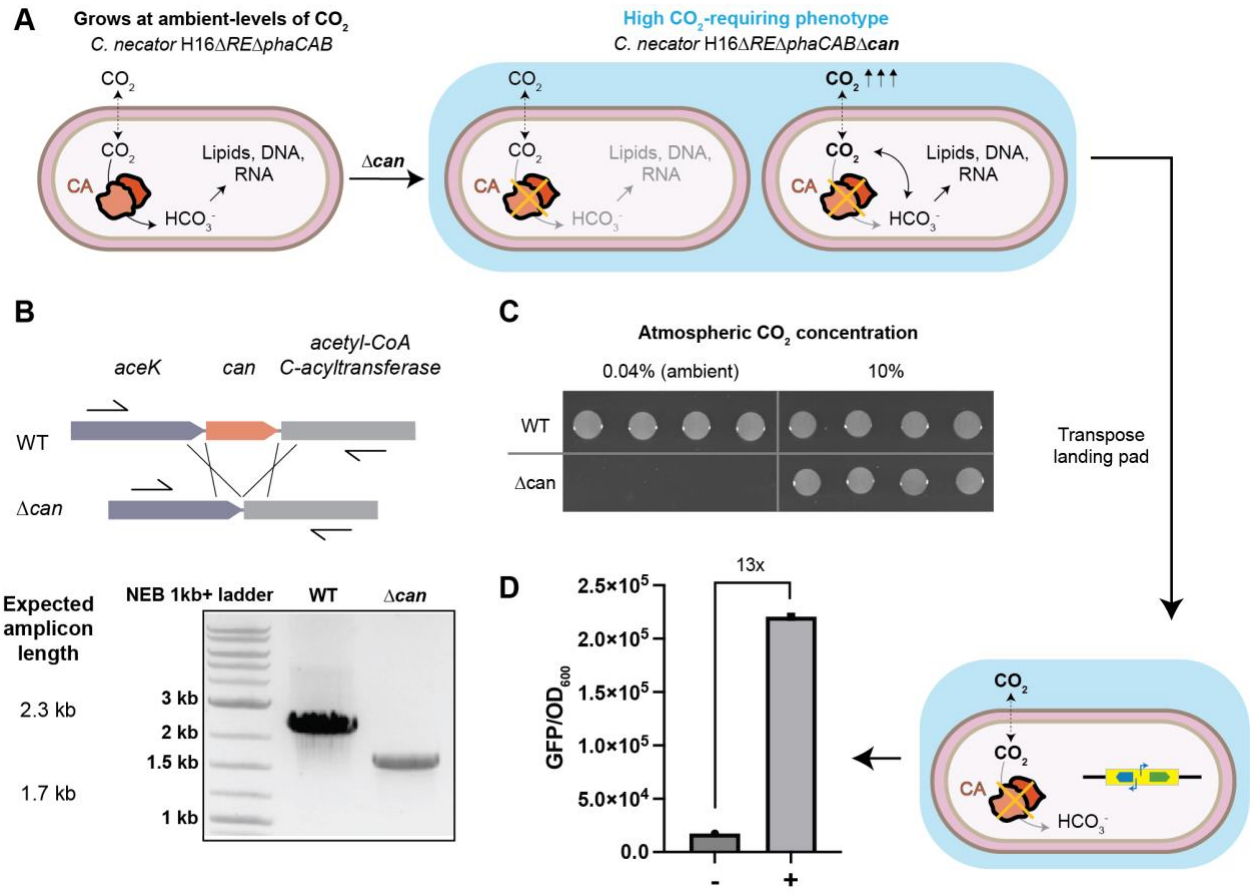


**Figure 4. Generating a *C. necator* strain with a high $CO_2$ requiring (HCR) phenotype.** (A) A landing pad was transconjucated into a *C. necator* strain exhibiting an HCR phenotype from the deletion of the carbonic anhydrase, *can*. (B) PCR amplification across the can locus in the H16 ΔREΔ*phaCAB*Δ*can* background to genotypically determine deletion of the carbonic anhydrase. (C) Growth phenotype of H16 ΔREΔ*phaCAB*Δ*can* strain under ambient and elevated (10%) concentrations of $CO_2$. (D) AraC/$P_{araBAD}$ landing pad was transconjugated into the H16 ΔREΔ*phaCAB*Δ*can* background. Fluorescence was measured 20 hours post treatment with 5 mM l-arabinose.

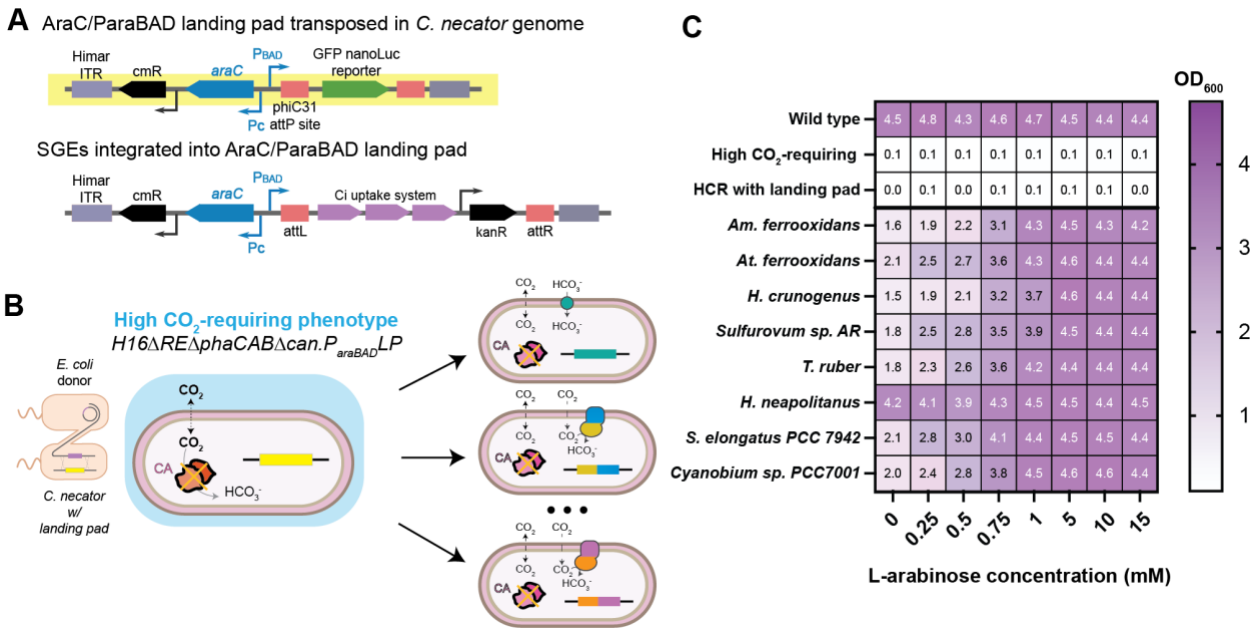


**Figure 5. Heterologous Ci uptake system expression recover HCR phenotype in heterotrophically cultured *C. necator*.** (A) Ci uptake system candidate pathways assembled into the pPath vector are integrated into the transposed landing pad via PhiC31 integrase activity. (B) Candidate Ci uptake systems were conjugated into the H16 ΔREΔ*phaCAB*Δ*can* background transposed with AraC/$P_{araBAD}$ landing pad. (C) $OD_{600}$ of Ci uptake system candidate carrying HCR strains cultivated at ambient air conditions (0.04% $CO_2$), 22 hours post induction with increasing concentrations of l-arabinose. Heatmap represents the average value of replicates.

| Species | Subunit | IMG gene ID | Length (bp) | Reference |
|---|---|---|---|---|
| *Acidimicrobium ferrooxidans* | CM | 644951280 | 4149 | [44] |
| *Acidithiobacillus ferrooxidans* | C | 642789231 | 1641 | |
| | M | 642789232 | 2478 | |
| *Hydrogenovibrio crunogenus* | C | 637785574 | 1557 | |
| | M | 637785573 | 2472 | |
| *Sulfurovumsp. strain AR* | C | 2620607600 | 1614 | |
| | M | 2620607602 | 729 | |
| | T | 2620607601 | 2880 | |
| *Thermocrinis ruber* | TC | 2512918850 | 2283 | |
| | M | 2512918849 | 2997 | |
| *Halothiobacillus neapolitanus* | DabB2 | 646382590 | 2484 | [45] |
| | DabA2 | 646382589 | 1656 | |
| *Synechococcusspp. PCC7942* | SbtA | 637799907 | 1122 | [46] |
| | SbtB | 637799908 | 315 | |
| *Cyanobium sp. PCC7001* | SbtA | 647590134 | 999 | |
| | SbtB | 647590133 | 315 | |

**Table 1. Inorganic carbon (Ci) uptake system candidates.** Identified Ci uptake systems reported to upregulate intracellular bicarbonate concentrations when expressed in *E. coli* from the literature. Systems are found in 1-, 2-, and 3-subunit configurations. For Ci uptake systems characterized in Schmid *et al.,* 2021, the subunits are annotated as a membrane-spanning protein (M subunit), a cytoplasmic protein (C subunit), and a tiny subunit (T subunit) that is encoded by a small gene that can be found between genes encoding the M and C subunits. The *A. ferrooxidans* CM is a fusion protein of the C and M subunits. Subunits are listed in the order that they are found in the native operon.

## Methods

### Plasmid construction:

Detailed information on plasmids is reported in Table S1. To generate inducible system variants, candidate inducible systems were assembled into the pLP-pcepA-himar-chlorR vector backbone via Gibson assembly using NEBuilder HiFi DNA assembly master mix (New England Biolabs). Ci uptake systems were assembled into the pPath-pcepA-integrase_v2 vector by Golden gate assembly using NEBridge Golden Gate Enzyme Mix (BsaI-HFv2) (NEB).

The *can* gene deletion plasmid was assembled by amplifying 750 bp upstream and 500 bp downstream of the *can* locus from *C. necator* genomic DNA using repliQa HiFi ToughMix (Quantabio) and Gibson assembly into the pK18msB vector (GenBank Accession # OK423783, Addgene Plasmid #177839) with NEBuilder HiFi DNA assembly master mix (NEB).

Ci uptake system genes were codon optimized for *C. necator* expression using the DeNovoDNA CDS calculator with the *C. necator* codon usage table[59,60]. Synthesis of genes encoding inducible systems and Ci uptake system candidates were performed by Twist Biosciences. Oligonucleotides were purchased from Integrated DNA Technologies with standard purification and desalting. Plasmids were transformed into *E. coli* TransforMax™ EC100D™ pir+ cells (Bioresearch technologies) and selected on LB agar plates containing the respective antibiotics. Colonies were screened by PCR and validated with whole plasmid sequencing (Plasmidsaurus).

### Media:

*E. coli* cultures were maintained in Lysogeny Broth (LB)-Lennox medium (LB, 10 g/L bacto tryptone, 5 g/L sodium chloride, 5 g/L yeast extract). *C. necator* cultures were maintained in a media mixture consisting of 50% LB-Lennox medium and 50% minimal salt media (MSM) (3.746 g/L $K_2HPO_4$, 1.156 g/L $KH_2PO_4$, 0.962 g/L $NH_4Cl$, 0.702 g/L NaCl, 66 mg/L citric acid, 16.68 mg/L $FeSO_4 \cdot 7H_2O$, 0.1 mg/L $ZnCl_2$, 0.03 mg/L $MnCl_2 \cdot 4H_2O$, 0.05 mg/L $CoCl_2 \cdot 6H_2O$, 0.07 mg/L $CuCl_2 \cdot 2H_2O$, 0.12 mg/L $NiCl_2 \cdot 6H_2O$, 0.03 mg/L $Na_2MoO_4 \cdot 2H_2O$, 0.05 mg/L $CrCl_3 \cdot 6H_2O$, 0.3 mg/L $H_3BO_3$, 11 mg/L $CaCl_2$, 240 mg/L $MgSO_4$) supplemented with 2 g/L fructose. *C. necator* was cultured on LB for agar plates. When antibiotic selection was required, kanamycin was used at 50 µg/mL for *E. coli* and 200 µg/ml for *C. necator*, chloramphenicol was used at 25 µg/mL for *E. coli* and 37.4 µg/mL for *C. necator*, and gentamycin was used at 15

μg/mL for *C. necator*. For culturing the auxotrophic *E. coli BW19851Δasd*, 100 μg/mL diaminopimelic acid (DAP) was supplemented. For inductions, l-arabinose, l-rhamnose, sodium salicylate, and sodium benzoate were prepared as 500 mM stock in water.

**Growth conditions:**

*E. coli* strains maintaining plasmids containing the heat inducible *pcepA* promoter were cultured at 30˚C to prevent expression of the transposase or integrase. The *C. necator* ΔREΔ*phaCAB*Δ*can* strain was cultured under 10% $CO_2$ at 30˚C in the Incu-Shaker $CO_2$ mini (Benchmark Scientific).

**Transformation conditions:**

For plasmid transformation into *E. coli*, we used the *E. coli* electroporation protocol described in Patel *et al*., 2022 [25]. To introduce landing pads and Ci uptake systems into *C. necator*, respective constructs were electroporated into the donor strain *E. coli BW19851Δasd* from Patel *et al*., 2022 for conjugation [25]. Interspecies conjugations were performed by preparing 25 mL late log donor and recipient strains, washing away selective antibiotics with PBS, mixing equal OD units of donor and recipient, concentrating the mixture 100x, and spotting 50 μL replicates of the mixture on solid LB + 100 μg/mL DAP. Conjugations proceeded for 24 hours at 30˚C, followed by a 1-hour incubation at 37˚C to induce transposase or integrase expression, and plated on selective DAP-free medium. Selection and counter-selection steps for *can* deletion in *C. necator* ΔREΔ*phaCAB* background were conducted under 10% $CO_2$. Conjugations of Ci uptake systems into *C. necator* ΔREΔ*phaCAB*Δ*can* were conducted under 10% $CO_2$.

**Calculation of transconjugation frequency:**

To calculate the transconjugation efficiency of the landing pad construct into *C. necator*, conjugants post 37˚C induction were serially diluted and plated on chloramphenicol 37.4 ug/mL agar plates and non-selective agar plates (**Figure 2B**). Plates were incubated at 30˚C for 48 hours. Colonies were observed for $10^0$ and $10^{-6}$ dilutions under selective and non-selective conditions, respectively. Transconjugation frequency was calculated by dividing number of colony forming units (CFUs) on selective media by number of CFUs on non-selective media multiplied by the dilution factor.

**Flow cytometry analysis:**

Fluorescent measurements were performed with the BD Symphony S6 cell sorter. For transconjugation populations, colonies on selective DAP-free plates were first lifted and grown for an hour at 30˚C. For individual clones, cell cultures were first grown overnight to saturation. These cultures were diluted 1:100 into inducer and cultured for an additional 12 hours. Cells were diluted 1:100 in PBS and loaded into the instrument. Quantification was done with FlowJo v10. Briefly, the cell population was gated with the forward scatter and side scatter channels, before quantifying fluorescent intensity in the FITC channel. FITC values were normalized by background subtraction of the wild type *C. necator* signal.

**Plate reader analysis:**

Fluorescent measurements for evaluating the performance of landing pad expression cassettes were performed on a BioTek Synergy H1 plate reader (Figure 2D-E, 3C-D, 4D, 5C, and S1-4). *C. necator* cultures were grown in 50% LB, 50% MSM 2 g/L fructose with the respective antibiotics overnight at 30˚C 225 rpm. Confluent cultures were diluted 1:50 into 50% LB, 50% MSM 2 g/L fructose in a black well clear bottom 96 well plate (100 µL per well). Absorbance at $OD_{600}$ and GFP fluorescence (485 nm ex, 528 nm em) values were measured kinetically every 20 minutes or for an endpoint ≤12 hours post induction. Cultures were grown at 30˚C under continuous double orbital shaking at 807 cpm in the plate reader. To quantify cell density - normalized fluorescence, GFP values were divided by $OD_{600}$ values. These values were further background subtracted using the average GFP/ $OD_{600}$ values of wildtype cells. For measuring growth of Ci uptake system expressing HCR strains, $OD_{600}$ was measured kinetically every 20 minutes or for an endpoint ≤12 hours post induction. $OD_{600}$ values were calibrated to $OD_{600}$ measurements at standard 1 cm path length (**Figure S5**).

**Gene deletion:**

Gene deletions were performed as previously described in Calvey *et al.,* 2022, with antibiotic selection and all following steps were conducted under 10% $CO_2$ for the *can* deletion[42].

**Genotyping:**

The *C. necator* wild type and ΔREΔ*phaCAB*Δ*can can* locus were genotyped from colony using repliQa HiFi ToughMix (Figure 4B). Results were analyzed on a 1% agarose gel stained with

ethidium bromide. Landing pad integration sites were identified by whole genome sequencing (Plasmidsaurus).

**Spotting assay:**

The *C. necator* ΔREΔ*phaCAB*Δ*can* was incubated under 0.04% (atmospheric $CO_2$ concentration) and 10% $CO_2$ to assess the HCR phenotype (Figure 4C). *C. necator* ΔREΔ*phaCAB*Δ*can* cultures were grown in 50 % LB, 50% MSM 2 g/L fructose overnight at 30˚C 225 rpm. 3 µL of the culture was spotted on LB agar plates, and separately incubated at 0.04% (atmospheric $CO_2$ concentration) and 10% $CO_2$ at 30˚C for 48 hours.

**Abbreviations**

aTc - anhydrotetracycline

Ci - inorganic carbon

HCR – high $CO_2$-requiring

**Author Information**

**Corresponding author**

Farren J. Isaacs - Department of Molecular, Cellular, and Developmental Biology, Department of Biomedical Engineering, Systems Biology Institute, Yale University, New Haven, CT, 06520, USA; https://orcid.org/0000-0001-8615-8236; Email: farren.isaacs@yale.edu

**Authors**

Akira K. Nakamura - Department of Molecular, Cellular, and Developmental Biology, Systems Biology Institute, Yale University, New Haven, CT, 06520, USA; https://orcid.org/0000-0001-8156-3216

Emily M. Fulk - Renewable Resources and Enabling Sciences Center, National Renewable Energy Laboratory, Golden, CO 80401, USA; https://orcid.org/0000-0002-1532-1398

Christopher W. Johnson - Renewable Resources and Enabling Sciences Center, National Renewable Energy Laboratory, Golden, CO 80401, USA; https://orcid.org/0000-0002-2979-4751

## Author Contribution

A.K.N. and F.J.I. conceived the experiments and directed the studies. A.K.N. conducted the experiments and analyzed data. E.M.F. and C.W.J. provided *C. necator* strains and expertise. A.K.N. and F.J.I. wrote the manuscript with revisions by E.M.F. and C.W.J.

## Conflict of Interest

F.J.I. is a co-inventor on a Yale patent application describing the original CAD-SGE technology. All other authors declare no competing financial interest.

## Supporting information

- Supplementary text, tables, figures and references (PDF)
- Source data (XLSX)

## Acknowledgment

We are grateful to members of the Isaacs lab, Rinehart lab, and members of the DE-FOA- DE-SC0023278 grant for their critical discussions and feedback. We thank Kenneth Nelson and Fiona Fenteany (Yale West Campus Analytical Core facility) for assistance with flow-cytometry experiments. We thank Biorender.com for providing illustrations for figures. We gratefully acknowledge funding from the Department of Energy BER Biosystems Design Program (DE-SC0023278).

## References


(1) van der Van, M.; Kobayashi, Y.; Diercks, R. Technology Roadmap: Energy and GHG Reductions in the Chemical Industry via Catalytic Processes. *Energy Technology Perspective* **2013**.

(2) Clomburg, J. M.; Crumbley, A. M.; Gonzalez, R. Industrial Biomanufacturing: The Future of Chemical Production. *Science*. 2017. https://doi.org/10.1126/science.aag0804.

(3) Nielsen, J.; Larsson, C.; van Maris, A.; Pronk, J. Metabolic Engineering of Yeast for Production of Fuels and Chemicals. *Current Opinion in Biotechnology*. 2013. https://doi.org/10.1016/j.copbio.2013.03.023.

(4) Keasling, J. D. Manufacturing Molecules through Metabolic Engineering. *Science*. 2010. https://doi.org/10.1126/science.1193990.

(5) Liew, F. E.; Nogle, R.; Abdalla, T.; Rasor, B. J.; Canter, C.; Jensen, R. O.; Wang, L.; Strutz, J.; Chirania, P.; De Tissera, S.; Mueller, A. P.; Ruan, Z.; Gao, A.; Tran, L.; Engle, N. L.; Bromley, J. C.; Daniell, J.; Conrado, R.; Tschaplinski, T. J.; Giannone, R. J.; Hettich, R. L.; Karim, A. S.; Simpson, S. D.; Brown, S. D.; Leang, C.; Jewett, M. C.; Köpke, M. Carbon-Negative Production of Acetone and Isopropanol by Gas Fermentation at Industrial Pilot Scale. *Nat Biotechnol* **2022**, *40* (3). https://doi.org/10.1038/s41587-021-01195-w.

(6) Scown, C. D. Prospects for Carbon-Negative Biomanufacturing. *Trends in Biotechnology*. 2022. https://doi.org/10.1016/j.tibtech.2022.09.004.

(7) Panich, J.; Fong, B.; Singer, S. W. Metabolic Engineering of Cupriavidus Necator H16 for Sustainable Biofuels from CO2. *Trends Biotechnol* **2021**, *39* (4), 412–424. https://doi.org/10.1016/J.TIBTECH.2021.01.001.

(8) Wang, Y.; Cui, L.; Ding, L.; Su, X.; Luo, H.; Huang, H.; Wang, Y.; Yao, B.; Zhang, J.; Wang, X. Unlocking the Potential of Cupriavidus Necator H16 as a Platform for Bioproducts Production from Carbon Dioxide. *World Journal of Microbiology and Biotechnology 2024 40:12* **2024**, *40* (12), 1–20. https://doi.org/10.1007/S11274-024-04200-X.

(9) Madison, L. L.; Huisman, G. W. Metabolic Engineering of Poly(3-Hydroxyalkanoates): From DNA to Plastic. *Microbiology and Molecular Biology Reviews* **1999**, *63* (1), 21–53. https://doi.org/10.1128/MMBR.63.1.21-53.1999/ASSET/8845D3C0-C28B-4989-8FB3-46BF2A21EAA5/ASSETS/GRAPHIC/MR0190002016.JPEG.

(10) Müller, J.; MacEachran, D.; Burd, H.; Sathitsuksanoh, N.; Bi, C.; Yeh, Y. C.; Lee, T. S.; Hillson, N. J.; Chhabra, S. R.; Singer, S. W.; Beller, H. R. Engineering of Ralstonia Eutropha H16 for Autotrophic and Heterotrophic Production of Methyl Ketones. *Appl Environ Microbiol* **2013**, *79* (14), 4433–4439. https://doi.org/10.1128/AEM.00973-13/SUPPL_FILE/ZAM999104544SO1.PDF.

(11) Crépin, L.; Lombard, E.; Guillouet, S. E. Metabolic Engineering of Cupriavidus Necator for Heterotrophic and Autotrophic Alka(e)Ne Production. *Metab Eng* **2016**, *37*, 92–101. https://doi.org/10.1016/J.YMBEN.2016.05.002.

(12) Lu, J.; Brigham, C. J.; Gai, C. S.; Sinskey, A. J. Studies on the Production of Branched-Chain Alcohols in Engineered Ralstonia Eutropha. *Appl Microbiol Biotechnol* **2012**, *96* (1), 283–297. https://doi.org/10.1007/S00253-012-4320-9/FIGURES/7.

(13) Krieg, T.; Sydow, A.; Faust, S.; Huth, I.; Holtmann, D. CO2 to Terpenes: Autotrophic and Electroautotrophic α-Humulene Production with Cupriavidus Necator. *Angewandte Chemie International Edition* **2018**, *57* (7), 1879–1882. https://doi.org/10.1002/ANIE.201711302.

(14) Weiler, J. R.; Jürgensen, N.; Cornejo Infante, M.; Knoll, M. T.; Gescher, J. Strain and Model Development for Auto- and Heterotrophic 2,3-Butanediol Production Using Cupriavidus Necator H16. *Biotechnology for Biofuels and Bioproducts* **2024**, *17* (1), 1–16. https://doi.org/10.1186/S13068-024-02549-7/TABLES/5.

(15) Windhorst, C.; Gescher, J. Efficient Biochemical Production of Acetoin from Carbon Dioxide Using Cupriavidus Necator H16. *Biotechnol Biofuels* **2019**, *12* (1), 1–11. https://doi.org/10.1186/S13068-019-1512-X/TABLES/1.

(16) Gascoyne, J. L.; Bommareddy, R. R.; Heeb, S.; Malys, N. Engineering Cupriavidus Necator H16 for the Autotrophic Production of (R)-1,3-Butanediol. *Metab Eng* **2021**, *67*, 262–276. https://doi.org/10.1016/J.YMBEN.2021.06.010.

(17) Garavaglia, M.; McGregor, C.; Bommareddy, R. R.; Irorere, V.; Arenas, C.; Robazza, A.; Minton, N. P.; Kovacs, K. Stable Platform for Mevalonate Bioproduction from CO2. *ACS Sustain Chem Eng* **2024**, *12* (36), 13486–13499. https://doi.org/10.1021/ACSSUSCHEMENG.4C03561/ASSET/IMAGES/LARGE/SC4C03561_0007.JPEG.

(18) Salinas, A.; McGregor, C.; Irorere, V.; Arenas-López, C.; Bommareddy, R. R.; Winzer, K.; Minton, N. P.; Kovács, K. Metabolic Engineering of Cupriavidus Necator H16 for Heterotrophic and Autotrophic Production of 3-Hydroxypropionic Acid. *Metab Eng* **2022**, *74*, 178–190. https://doi.org/10.1016/J.YMBEN.2022.10.014.

(19) Pan, H.; Wang, J.; Wu, H.; Li, Z.; Lian, J. Synthetic Biology Toolkit for Engineering Cupriviadus Necator H16 as a Platform for CO2 Valorization. *Biotechnol Biofuels* **2021**, *14* (1), 1–20. https://doi.org/10.1186/S13068-021-02063-0/FIGURES/5.

(20) Lenz, O.; Friedrich, B. A Novel Multicomponent Regulatory System Mediates H2 Sensing in Alcaligenes Eutrophus. *Proc Natl Acad Sci U S A* **1998**, *95* (21). https://doi.org/10.1073/pnas.95.21.12474.

(21) Marx, C. J. Development of a Broad-Host-Range SacB-Based Vector for Unmarked Allelic Exchange. *BMC Res Notes* **2008**, *1* (1), 1–8. https://doi.org/10.1186/1756-0500-1-1/TABLES/1.

(22) Kung, S. H.; Retchless, A. C.; Kwan, J. Y.; Almeida, R. P. P. Effects of DNA Size on Transformation and Recombination Efficiencies in Xylella Fastidiosa. *Appl Environ Microbiol* **2013**, *79* (5). https://doi.org/10.1128/AEM.03525-12.

(23) Bryant, J. A.; Sellars, L. E.; Busby, S. J. W.; Lee, D. J. Chromosome Position Effects on Gene Expression in Escherichia Coli K-12. *Nucleic Acids Res* **2014**, *42* (18), 11383–11392. https://doi.org/10.1093/NAR/GKU828.

(24) Martínez-García, E.; Aparicio, T.; De Lorenzo, V.; Nikel, P. I. Engineering Gram-Negative Microbial Cell Factories Using Transposon Vectors. *Methods in Molecular Biology* **2017**, *1498*, 273–293. https://doi.org/10.1007/978-1-4939-6472-7_18/FIGURES/1.

(25) Patel, J.; Oh, J.; Wang, S.; Crawford, J.; Isaacs, F. In Brief Cross-Kingdom Expression of Synthetic Genetic Elements Promotes Discovery of Metabolites in the Human Microbiome. *Cell* **2022**, *185*. https://doi.org/10.1016/j.cell.2022.03.008.

(26) Wang, G.; Zhao, Z.; Ke, J.; Engel, Y.; Shi, Y. M.; Robinson, D.; Bingol, K.; Zhang, Z.; Bowen, B.; Louie, K.; Wang, B.; Evans, R.; Miyamoto, Y.; Cheng, K.; Kosina, S.; De Raad, M.; Silva, L.; Luhrs, A.; Lubbe, A.; Hoyt, D. W.; Francavilla, C.; Otani, H.; Deutsch, S.; Washton, N. M.; Rubin, E. M.; Mouncey, N. J.; Visel, A.; Northen, T.; Cheng, J. F.; Bode, H. B.; Yoshikuni, Y. CRAGE Enables Rapid Activation of Biosynthetic Gene Clusters in Undomesticated Bacteria. *Nat Microbiol* **2019**, *4* (12). https://doi.org/10.1038/s41564-019-0573-8.

(27) Tcherkez, G. G. B.; Farquhar, G. D.; Andrews, T. J. Despite Slow Catalysis and Confused Substrate Specificity, All Ribulose Bisphosphate Carboxylases May Be Nearly Perfectly Optimized. *Proceedings of the National Academy of Sciences* **2006**, *103* (19), 7246–7251. https://doi.org/10.1073/PNAS.0600605103.

(28) Wilde, E.; Schlegel, H. G. Oxygen Tolerance of Strictly Aerobic Hydrogen-Oxidizing Bacteria. *Antonie Van Leeuwenhoek* **1982**, *48* (2), 131–143. https://doi.org/10.1007/BF00405198/METRICS.

(29) Satagopan, S.; Tabita, F. R. RubisCO Selection Using the Vigorously Aerobic and Metabolically Versatile Bacterium Ralstonia Eutropha. *FEBS J* **2016**, *283* (15), 2869–2880. https://doi.org/10.1111/FEBS.13774.

(30) Hennacy, J. H.; Jonikas, M. C. Prospects for Engineering Biophysical CO2 Concentrating Mechanisms into Land Plants to Enhance Yields. *Annu Rev Plant Biol* **2020**, *71*, 461–485. https://doi.org/10.1146/ANNUREV-ARPLANT-081519-040100.

(31) Moroney, J. V.; Ynalvez, R. A. Proposed Carbon Dioxide Concentrating Mechanism in Chlamydomonas Reinhardtii. *Eukaryot Cell* **2007**, *6* (8), 1251–1259. https://doi.org/10.1128/EC.00064-07/ASSET/46103945-16FD-4949-8871-3357EC1EA572/ASSETS/GRAPHIC/ZEK0080729220003.JPEG.

(32) Badger, M. R.; Price, G. D. CO2 Concentrating Mechanisms in Cyanobacteria: Molecular Components, Their Diversity and Evolution. *J Exp Bot* **2003**, *54* (383), 609–622. https://doi.org/10.1093/JXB/ERG076.

(33) Flamholz, A. I.; Dugan, E.; Panich, J.; Desmarais, J. J.; Oltrogge, L. M.; Fischer, W. W.; Singer, S. W.; Savage, D. F. Trajectories for the Evolution of Bacterial CO2-Concentrating Mechanisms. *Proceedings of the National Academy of Sciences* **2022**, *119* (49), e2210539119. https://doi.org/10.1073/PNAS.2210539119.

(34) Panich, J.; Toppari, E.; Tejedor-Sanz, S.; Fong, B.; Dugan, E.; Chen, Y.; Petzold, C. J.; Zhao, Z.; Yoshikuni, Y.; Savage, D. F.; Singer, S. W. Functional Plasticity of HCO3– Uptake and CO2 Fixation in Cupriavidus Necator H16. *Bioresour Technol* **2024**, *410*, 131214. https://doi.org/10.1016/J.BIORTECH.2024.131214.

(35) Alagesan, S.; Hanko, E. K. R.; Malys, N.; Ehsaan, M.; Winzer, K.; Minton, N. P. Functional Genetic Elements for Controlling Gene Expression in Cupriavidus Necator H16. *Appl Environ Microbiol* **2018**, *84* (19). https://doi.org/10.1128/AEM.00878-18/SUPPL_FILE/ZAM019188767S1.PDF.

(36) Hanko, E. K. R.; Paiva, A. C.; Jonczyk, M.; Abbott, M.; Minton, N. P.; Malys, N. A Genome-Wide Approach for Identification and Characterisation of Metabolite-Inducible Systems. *Nature Communications 2020 11:1* **2020**, *11* (1), 1–14. https://doi.org/10.1038/s41467-020-14941-6.

(37) Scholz, S. A.; Lindeboom, C. D.; Freddolino, P. L. Genetic Context Effects Can Override Canonical Cis Regulatory Elements in Escherichia Coli. *Nucleic Acids Res* **2022**, *50* (18), 10360–10375. https://doi.org/10.1093/NAR/GKAC787.

(38) Brooks, A. N.; Hughes, A. L.; Clauder-Münster, S.; Mitchell, L. A.; Boeke, J. D.; Steinmetz, L. M. Transcriptional Neighborhoods Regulate Transcript Isoform Lengths and Expression Levels. *Science (1979)* **2022**, *375* (6584). https://doi.org/10.1126/science.abg0162.

(39) Li, H.; Liao, J. C. A Synthetic Anhydrotetracycline-Controllable Gene Expression System in Ralstonia Eutropha H16. *ACS Synth Biol* **2015**, *4* (2), 101–106. https://doi.org/10.1021/SB4001189/SUPPL_FILE/SB4001189_SI_001.PDF.

(40) Mishra, S.; Perkovich, P. M.; Mitchell, W. P.; Venkataraman, M.; Pfleger, B. F. Expanding the Synthetic Biology Toolbox of Cupriavidus Necator for Establishing Fatty Acid Production. *J Ind Microbiol Biotechnol* **2024**, *51*. https://doi.org/10.1093/jimb/kuae008.

(41) Xiong, B.; Li, Z.; Liu, L.; Zhao, D.; Zhang, X.; Bi, C. Genome Editing of Ralstonia Eutropha Using an Electroporation-Based CRISPR-Cas9 Technique. *Biotechnol Biofuels* **2018**, *11* (1), 1–9. https://doi.org/10.1186/S13068-018-1170-4/TABLES/4.

(42) Calvey, C. H.; Sànchez i Nogué, V.; White, A. M.; Kneucker, C. M.; Woodworth, S. P.; Alt, H. M.; Eckert, C. A.; Johnson, C. W. Improving Growth of Cupriavidus Necator H16 on Formate Using Adaptive Laboratory Evolution-Informed Engineering. *Metab Eng* **2022**. https://doi.org/10.1016/J.YMBEN.2022.10.016.

(43) Wang, J.; Yu, H. Q. Biosynthesis of Polyhydroxybutyrate (PHB) and Extracellular Polymeric Substances (EPS) by Ralstonia Eutropha ATCC 17699 in Batch Cultures. *Appl Microbiol Biotechnol* **2007**, *75* (4). https://doi.org/10.1007/s00253-007-0870-7.

(44) Schmid, S.; Chaput, D.; Breitbart, M.; Hines, R.; Williams, S.; Gossett, H. K.; Parsi, S. D.; Peterson, R.; Whittaker, R. A.; Tarver, A.; Scott, K. M. Dissolved Inorganic Carbon-Accumulating Complexes from Autotrophic Bacteria from Extreme Environments. *J Bacteriol* **2021**, *203* (23). https://doi.org/10.1128/JB.00377-21/SUPPL_FILE/JB.00377-21-S0001.PDF.

(45) Desmarais, J. J.; Flamholz, A. I.; Blikstad, C.; Dugan, E. J.; Laughlin, T. G.; Oltrogge, L. M.; Chen, A. W.; Wetmore, K.; Diamond, S.; Wang, J. Y.; Savage, D. F. DABs Are Inorganic Carbon Pumps Found throughout Prokaryotic Phyla. *Nature Microbiology 2019 4:12* **2019**, *4* (12), 2204–2215. https://doi.org/10.1038/s41564-019-0520-8.

(46) Du, J.; Förster, B.; Rourke, L.; Howitt, S. M.; Price, G. D. Characterisation of Cyanobacterial Bicarbonate Transporters in E. Coli Shows That SbtA Homologs Are Functional in This Heterologous Expression System. *PLoS One* **2014**, *9* (12), e115905. https://doi.org/10.1371/JOURNAL.PONE.0115905.

(47) Merlin, C.; Masters, M.; McAteer, S.; Coulson, A. Why Is Carbonic Anhydrase Essential to Escherichia Coli? *J Bacteriol* **2003**, *185* (21), 6415–6424. https://doi.org/10.1128/JB.185.21.6415-6424.2003/ASSET/504030E8-3449-4422-A92C-579EDFC9A8A5/ASSETS/GRAPHIC/JB2130613007.JPEG.

(48) Gai, C. S.; Lu, J.; Brigham, C. J.; Bernardi, A. C.; Sinskey, A. J. Insights into Bacterial CO2 Metabolism Revealed by the Characterization of Four Carbonic Anhydrases in Ralstonia Eutropha H16. *AMB Express* **2014**, *4* (1), 2. https://doi.org/10.1186/2191-0855-4-2.

(49) Huang, W.; Wilks, A. A Rapid Seamless Method for Gene Knockout in Pseudomonas Aeruginosa. *BMC Microbiol* **2017**, *17* (1). https://doi.org/10.1186/s12866-017-1112-5.

(50) Merrick, C. A.; Zhao, J.; Rosser, S. J. Serine Integrases: Advancing Synthetic Biology. *ACS Synth Biol* **2018**, *7* (2). https://doi.org/10.1021/acssynbio.7b00308.

(51) Elmore, J. R.; Dexter, G. N.; Baldino, H.; Huenemann, J. D.; Francis, R.; Peabody, G. L. V.; Martinez-Baird, J.; Riley, L. A.; Simmons, T.; Coleman-Derr, D.; Guss, A. M.; Egbert, R. G. High-Throughput Genetic Engineering of Nonmodel and Undomesticated Bacteria via Iterative Site-Specific Genome Integration. *Sci Adv* **2023**, *9* (10). https://doi.org/10.1126/sciadv.ade1285.

(52) Federici, F.; Luppino, F.; Aguilar-Vilar, C.; Mazaraki, M. E.; Petersen, L. B.; Ahonen, L.; Nikel, P. I. CIFR (Clone–Integrate–Flip-out–Repeat): A Toolset for Iterative Genome and Pathway Engineering of Gram-Negative Bacteria. *Metab Eng* **2025**, *88*, 180–195. https://doi.org/10.1016/J.YMBEN.2025.01.001.

(53) Kovach, M. E.; Elzer, P. H.; Steven Hill, D.; Robertson, G. T.; Farris, M. A.; Roop, R. M.; Peterson, K. M. Four New Derivatives of the Broad-Host-Range Cloning Vector PBBR1MCS, Carrying Different Antibiotic-Resistance Cassettes. *Gene* **1995**, *166* (1), 175–176. https://doi.org/10.1016/0378-1119(95)00584-1.

(54) Balbás, P. Understanding the Art of Producing Protein and Nonprotein Molecules in Escherichia Coli. *Applied Biochemistry and Biotechnology - Part B Molecular Biotechnology*. 2001. https://doi.org/10.1385/MB:19:3:251.

(55) Wang, Z.; Pan, H.; Ni, S.; Li, Z.; Lian, J. Establishing CRISPRi for Programmable Gene Repression and Genome Evolution in Cupriavidus Necator. *ACS Synth Biol* **2024**, *13* (3). https://doi.org/10.1021/acssynbio.3c00664.

(56) Valle, S. Della; Orsi, E.; Creutzburg, S. C. A.; Jansen, L. F. M.; Pentari, E.-N.; Beisel, C. L.; Steel, H.; Nikel, P. I.; Staals, R. H. J.; Claassens, N. J.; Oost, J. van der; Huang, W. E.; Patinios, C. Streamlined and Efficient Genome Editing in Cupriavidus Necator H16 Using an Optimised SIBR-Cas System. *bioRxiv* **2024**, 2024.11.24.625072. https://doi.org/10.1101/2024.11.24.625072.

(57) Wang, H. H.; Isaacs, F. J.; Carr, P. A.; Sun, Z. Z.; Xu, G.; Forest, C. R.; Church, G. M. Programming Cells by Multiplex Genome Engineering and Accelerated Evolution. *Nature* **2009**, *460* (7257). https://doi.org/10.1038/nature08187.

(58) Gallagher, R. R.; Li, Z.; Lewis, A. O.; Isaacs, F. J. Rapid Editing and Evolution of Bacterial Genomes Using Libraries of Synthetic DNA. *Nature Protocols 2014 9:10* **2014**, *9* (10), 2301–2316. https://doi.org/10.1038/nprot.2014.082.

(59) Halper, S. M.; Hossain, A.; Salis, H. M. Synthesis Success Calculator: Predicting the Rapid Synthesis of DNA Fragments with Machine Learning. *ACS Synth Biol* **2020**, *9* (7), 1563–1571. https://doi.org/10.1021/ACSSYNBIO.9B00460/SUPPL_FILE/SB9B00460_SI_004.XLSX.

(60) Reis, A. C.; Salis, H. M. An Automated Model Test System for Systematic Development and Improvement of Gene Expression Models. *ACS Synth Biol* **2020**, *9* (11), 3145–3156. https://doi.org/10.1021/ACSSYNBIO.0C00394/SUPPL_FILE/SB0C00394_SI_006.XLSX.

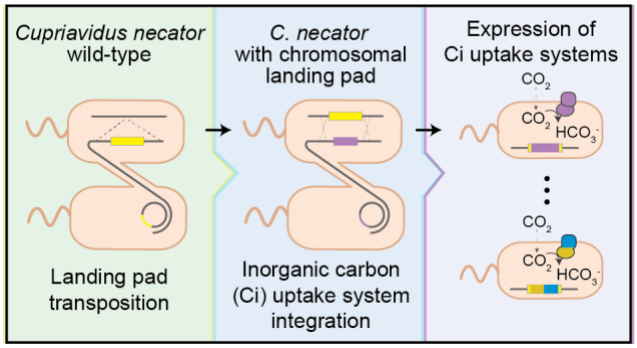


**For Table of Contents Only**

**Synthetic genetic elements enable rapid characterization of inorganic carbon uptake systems in *Cupriavidus necator* H16**

Akira K. Nakamura, Emily M. Fulk, Christopher W. Johnson, and Farren J. Isaacs